Applicable Analysis
Vol. 83, No. 2, February 2004, pp. 199–215

Taylor & Francis
Taylor & Francis Group

The Raised-Cosine Wavelets in Computerized Tomography

TATIANA SOLESKI* and GILBERT WALTER†

Department of Mathematical Sciences, University of Wisconsin-Milwaukee, P.O. Box 413, Milwaukee, WI 53201-0413, USA

Communicated by R.P. Gilbert

(Received 27 July 2003)

In Computerized Tomography (CT), an image must be recovered from its sampled projections in the form of values of the Radon transform. In this work a method of recovering the image is based on the properties of the raised-cosine wavelet. This wavelet has a closed form which allows for certain precomputations and avoids convolution. The rate of convergence of the resulting algorithm to the image density function is found under suitable hypotheses. This algorithm is then tested on the standard Shepp–Logan image.

Keywords: Raised-cosine wavelets; Sampling theory; Radon transform; Computerized tomography

AMS Subject Classifications: 42C40; 94A08

1. INTRODUCTION

One of the many applications of wavelet theory is in computerized tomography (CT) in which an image must be recovered from its sampled projections in the form of the Radon transform data. In this article we present a new wavelet based reconstruction algorithm that is computationally effective while providing a high quality reconstructed image. The wavelets used are the so called raised-cosine wavelets based on certain pulses widely used in digital communications and signal processing. These wavelets and the corresponding scaling function have a simple closed form described by Walter and Zhang [23].

More generally, we consider ways to reconstruct a function from its samples and the interplay between wavelets, sampling theory, and the Radon transform. One of the first (and, probably, the most famous) results of sampling theory was the Shannon sampling theorem [15] which allows one to reconstruct a bandlimited signal

*Corresponding author. E-mail: tigol@uwm.edu
†E-mail: ggw@uwm.edu

ISSN 0003-6811 print: ISSN 1563-504X online
DOI: 10.1080/00036810310001632862

from its sampled values. The various extensions of this result such as nonuniform sampling and derivative sampling [11] have been obtained for both bandlimited and non-bandlimited signals. Sampling theorems were also shown to hold in wavelet subspaces by Walter [21,22] and Daubechies [5] and later by Aldroubi [1] and Unser *et al.* [17,18]. An excellent review of these methods can be found in [19].

A number of wavelet-based formulae have been proposed in the last few years to invert the Radon transform beginning with the work of Holschneider [10] in 1991 and Kaiser and Streater [13] in 1992. In 1992 Walnut [20] proposed an inversion formula based on the continuous wavelet transform. In 1992 his ideas were used by DeStefano and Olson [8] who implemented a numerical algorithm that allows one to reconstruct a local region of the image by using only the local data. In their 1994 paper, Berenstein and Walnut [3] gave formulae that relate the Radon transform and its inverse to various wavelet transforms. In 1997, in the modified backprojection algorithm, the usual filter was replaced by the wavelet ramp filter to reconstruct the wavelet coefficients of the object function [2]. In 2000, Donoho [9] used a Meyer type wavelet to construct special functions, called ridgelets, that give good approximation to the object functions with singularities along the lines.

These wavelet methods have the advantage that they are faster and in some cases can be applied with only local data. Most of these approaches use a continuous two-dimensional wavelet transform. Typically, the density function $f(x, y)$ of the image cross section is transformed by this wavelet transform to which the Radon transform is then applied. Since the two transforms commute, this may be approximated by the wavelet transform of the observation. The Radon transform is then inverted to obtain an approximation to the wavelet transform of the density function, which in turn may be used to approximate the density function itself. Discrete versions of this have also been tried and have usually used the two-dimensional Daubechies [5] or similar scaling functions and wavelets with compact support.

In this work we adopt a different approach which uses the wavelet approximation in the Radon transform domain. We also use sampling function as our scaling function in order to avoid integration. This approach enables us to make a number of one-time calculations which may then be stored for future calculations.

The work closest to ours in spirit is [2]. In order to reconstruct a local region of the image, the filtering step is implemented in the Fourier domain by multiplying the usual filter by the Fourier transform of a two-dimensional wavelet function. Then the backprojection step follows, and the result is the wavelet transform of the image function from which f itself can be reconstructed by using the inverse wavelet transform. The global results obtained there are comparable to ours, but the computational requirements seem to be greater. However, no systematical analysis has been made.

This article is organized as follows. Section 2, in addition to the brief introduction to the subject of CT, contains elements of wavelet theory as well as some definitions and important results from other sources which are used throughout. In Section 3, we present a reconstruction algorithm based on the raised-cosine spectrum function derived by Walter and Zhang [23]. Related wavelets are bandlimited and, unlike most of the wavelet families, have a simple closed form. Convergence theorems are proven for both the projection function and the object function and the rates of convergence are given. Computer simulations illustrating performance of the proposed algorithm are demonstrated for the well-known Shepp–Logan "head phantom."

2. WAVELETS AND COMPUTERIZED TOMOGRAPHY

In this section, we briefly mention some definitions, results, and notations from wavelet theory with particular emphasis on the raised-cosine wavelets.

2.1 Elements of Wavelet Theory

Wavelets constitute a Riesz basis of $L^2(\mathbf{R})$ consisting of translations and dilations of a single function $\psi(t)$ called a "mother wavelet":

$$\psi_{m,n}(t) = 2^{m/2}\psi(2^m t - n), \quad m, n \in \mathbf{Z}.$$

In certain cases these functions $\psi_{m,n}$ are orthonormal as well. The existence of a wavelet basis is not obvious. One usually begins with a so called scaling function $\phi(t)$ which is assumed to be in S^r, the Schwartz space of rapidly decreasing C^r – functions on $\mathbf{R}$, i.e., functions that satisfy $|\theta^{(k)}(t)| \le C_{p,k}(1 + |t|)^{-p}$ for $p = 0, 1, 2, \ldots$, $k = 0, 1, 2, \ldots, r$, and any $t \in \mathbf{R}$.

The construction of ϕ is closely related to the concept of MultiResolutional Analysis (MRA) of $L^2(\mathbf{R})$, i.e., a nested sequence of closed subspaces $\{V_m\}_{m\in\mathbf{Z}}$ such that

(i) $\cdots \subseteq V_{-1} \subseteq V_0 \subseteq V_1 \subseteq \cdots$
(ii) $f(t) \in V_m$ if and only if $f(2t) \in V_{m+1}$, $m \in \mathbf{Z}$
(iii) $\bigcap_m V_m = 0$, $\overline{\bigcup_m V_m} = L^2(\mathbf{R})$.

If, in addition, $\{\phi(t-n)\}_{n\in\mathbf{Z}}$ is an orthonormal basis of V_0, we say that $\{V_m\}$ is associated with ϕ. This orthonormality condition is often formulated in terms of $\hat{\phi}$, the Fourier transform of ϕ:

$$\sum_n |\hat{\phi}(\omega + 2\pi k)|^2 = 1.$$

The condition (ii) means that $\{\sqrt{2}\phi(2t-n)\}$ is an orthonormal basis of V_1. Therefore, there exists a sequence $\{c_k\} \in \ell^2$ such that $\phi(t) = \sum_k c_k \phi(2t-k)$. This is called the dilation equation.

If $\{\phi(t-n)\}$ is an orthonormal basis of V_0 then the mother wavelet $\psi(t)$ can be obtained by

$$\psi(t) = \sum_k c_{1-k}(-1)^k \psi(2t-k),$$

where $\{c_k\}$ are the coefficients of the dilation equation [6].

One of the examples of a scaling function is the Shannon scaling function $\phi_S(t) = (\sin \pi t)/\pi t$, which in the frequency domain is given by

$$\hat{\phi}_S(\omega) = \begin{cases} 1, & |\omega| \le \pi \\ 0, & \text{otherwise.} \end{cases}$$

Despite the fact that $\phi_S \notin S'$ due to a slow decay at infinity, it is extremely useful in a number of applications because of its sampling property:

$$f(t) = \sum_n f(n) \frac{\sin \pi(t-n)}{\pi(t-n)}$$

for any continuous function $f \in L^2(\mathbf{R})$ such that $\operatorname{supp} \hat{f} = [-\pi, \pi]$. The formula above is referred to as the Shannon sampling theorem [15].

Various other approaches have been used to construct a scaling function that meets all the requirements for an MRA [5,21]. Some have compact support while others are bandlimited as is ϕ_S.

Throughout the article the following definitions and notations from functional analysis are used.

The *Fourier transform* of a function $f \in L^1(-\infty, \infty)$ is defined to be

$$F(f) = \hat{f}(\omega) = \int_{-\infty}^{\infty} f(t) e^{-i\omega t}\, dt, \quad \omega \in \mathbf{R}.$$

For $\hat{f} \in L^1$, the *inverse Fourier transform* is defined as $F^{-1}(\hat{f}) = \check{\hat{f}}(t) = (1/2\pi) \int_{-\infty}^{\infty} \hat{f}(t) e^{i\omega t} d\omega$. If $f, g \in L^2$, Parseval's equality holds: $\langle f, g \rangle = (1/2\pi) \langle \hat{f}, \hat{g} \rangle$. A *tempered distribution* is an element of the dual space S' of the Schwartz space S of rapidly decreasing infinitely differentiable functions. Convergence in S of a sequence $\{\theta_n\}$ is defined as $x^p \theta_n^{(q)}(x) \to 0$ uniformly on $\mathbf{R}$ for each $p, q = 0, 1, 2, \ldots$. The space S' consists of all continuous linear functionals on S. Since S is closed under the Fourier transform, the Fourier transform of a tempered distribution T can be defined as follows:

$$\langle \hat{T}, \theta \rangle = \langle T, \hat{\theta} \rangle \quad \text{for any } \theta \in S.$$

It follows that $F(S') \subseteq S'$ and, in fact, it can be shown that $F(S') = S'$.

For all $\alpha \in \mathbf{R}$, the *delta function* $\delta_\alpha \in S'$ is defined as $\langle \delta_\alpha, \theta \rangle = \theta(\alpha)$ for $\theta \in S$. It is easy to see that $F(\delta_\alpha) = e^{-i\omega\alpha}$ and that $F^{-1}(\delta_\alpha) = 1/2\pi e^{i\omega\alpha}$. The *Poisson summation formula*: if a function ϕ is such that $\phi(t) = O(1 + |x|)^{-1-\varepsilon}$ and $\hat{\phi}(\omega) = O(1 + |\omega|)^{-1-\varepsilon}$ for some $\varepsilon > 0$ then

$$\sum_k \hat{\phi}(\omega + 2\pi k) = \sum_n \phi(-n) e^{i\omega n}.$$

It follows that ϕ is a sampling function (i.e., $\phi(0) = 1$ and $\phi(n) = 0$ otherwise for any $n \in \mathbf{Z}$) if and only if $\sum_k \hat{\phi}(\omega + 2\pi k) = 1$. The *periodic delta function* is defined as $\delta^*(\omega) = \sum_{k \in \mathbf{Z}} \delta(\omega - 2\pi k)$. Since δ is the Fourier transform of $1/(2\pi)$, a constant function, by an extension of the Poisson summation formula to S' we obtain $\delta^*(\omega) = (1/2\pi) \sum_n e^{i\omega n}$ in S'.

2.2 Mathematical Model of Computerized Tomography

The subject of CT deals with the cross-sectional imaging of an object from projection data collected by illuminating it by X-rays from many different angles. This has been

one of the most significant developments in medical imaging since the time of Roentgen (1895), and enables a medical practitioner to examine soft tissues as well as bones.

Two types of projection are possible. The simplest one is a parallel beam projection, and could be attained by moving the source and the detector along parallel lines on the opposite sides of an object. Another type is a so called fan-beam projection, and can be obtained if a single beam source is placed in a fixed position relatively to a line of the detectors. A fast and efficient algorithm [12] can be applied to convert the fan-beam projection data into equivalent parallel projections. This enables one to use a reconstruction algorithm designed for parallel scanning geometry. For this reason the algorithm presented in this work is developed for parallel projection data.

Let $f(x, y)$ be a two-dimensional density function of the object which is usually called the object function, or the image function. Then projection data $P_\theta(t)$ are represented by the line integrals

$$P_\theta(t) = \iint_{\mathbf{R}^2} f(x, y)\delta(x\cos\theta + y\sin\theta - t)\,dx\,dy,$$

where δ is the one-dimensional Dirac delta-function and $t = x\cos\theta + y\sin\theta$ is the equation of a line along which the projection has been measured. Mathematically, this is exactly the Radon transform $R_\theta f(t)$ of the object function. More details on the theory and applications of the Radon transform can be found in [7]. Thus, the problem of reconstructing a function from its profile at various angles is a Radon transform inversion problem.

The most popular inversion formula is based on the Fourier Slice theorem [12]:

$$\hat{R}_\theta f(\omega) = \hat{f}(\omega\cos\theta, \omega\sin\theta),$$

where $\hat{R}_\theta f$ and $\hat{f}$ denote the Fourier transform of $R_\theta f$ and f, respectively. In other words, the one-dimensional Fourier transform of the projection function gives the two-dimensional Fourier transform of the object function along a radial line. If projections are known at enough angles, the object function can be recovered by using an approximation to the inverse Fourier transform

$$f(x, y) = \frac{1}{(2\pi)^2}\iint_{\mathbf{R}^2} \hat{f}(u, v)e^{i(ux+vy)}\,du\,dv, \tag{1}$$

where $u = \omega\cos\theta, v = \omega\sin\theta$. By using polar coordinates in the frequency domain, (1) can be rewritten as

$$f(x, y) = \frac{1}{(2\pi)^2}\int_0^\pi \int_{-\infty}^{+\infty} \hat{R}_\theta f(\omega)e^{i\omega(x\cos\theta + y\sin\theta)}|\omega|\,d\omega\,d\theta, \tag{2}$$

which is called the backprojection formula. Two integrals in (2) are often separated to give a filter with transfer function $|\omega|$,

$$\hat{Q}_\theta(\omega) = \hat{R}_\theta f(\omega)|\omega|,$$

whose inverse Fourier transform is the inner integral in (2) evaluated at $t = x\cos\theta + y\sin\theta$. This is followed by an averaging operator (backprojection) that recovers the object function,

$$f(x, y) = \frac{1}{2\pi}\int_0^{\pi} Q_\theta(t)\, d\theta,$$

In classical implementations, the transfer function $|\omega|$ is usually multiplied by a smoothing window $W(\omega)$ to make inversion of $\hat{Q}_\theta$ possible and obtain

$$Q_\theta(t) = (R_\theta f * h)(t),$$

where $h(t)$ is the inverse Fourier transform of $H(\omega) = |\omega| W(\omega)$ and "$*$" denotes convolution. One example of an effective filter function is obtained by introducing a cosine-weighted function into $|\omega|$:

$$H(\omega) = \begin{cases} |\omega| \cos(\pi\omega/2\omega_0), & |\omega| \le \omega_0 \\ 0 & \text{otherwise,} \end{cases}$$

where ω_0 is the highest frequency in the projection [4].

2.3 The Raised-Cosine Wavelets

The raised-cosine wavelets are particular cases of the Meyer type wavelets. There are several different forms but all are bandlimited and the one we use will have cubic polynomial decay in time. But unlike almost all known wavelet families, they have a simple analytic form. This remarkable property makes them very attractive for applications as it can reduce or even eliminate some numerical calculations needed otherwise.

The raised-cosine spectrum function is defined by means of its Fourier transform as follows:

$$\hat{\phi}(\omega) = \begin{cases} 1, & 0 \le |\omega| \le \pi(1-\beta) \\ \dfrac{1}{2}\left\{1 + \cos\left[\dfrac{1}{2\beta}(|\omega| - \pi(1-\beta))\right]\right\}, & \pi(1-\beta) \le |\omega| \le \pi(1+\beta), \\ 0, & |\omega| \ge \pi(1+\beta) \end{cases} \tag{3}$$

for any $0 < \beta \le 1/3$. We shall use the value $\beta = 1/4$. Then (3) becomes

$$\hat{\phi}(\omega) = \begin{cases} 1, & 0 \le |\omega| \le \dfrac{3\pi}{4} \\ \dfrac{1}{2} + \dfrac{1}{2}\cos\left(2|\omega| - \dfrac{3\pi}{2}\right), & \dfrac{3\pi}{4} \le |\omega| \le \dfrac{5\pi}{4}. \\ 0, & |\omega| \ge \dfrac{5\pi}{4} \end{cases}$$

The inverse Fourier transform is also easily calculated in closed form. It is

$$\phi(t) = \frac{2\sin((3\pi/4)t) + 2\sin((5\pi/4)t)}{\pi t(4 - t^2)}.$$

The graphs of ϕ and $\hat{\phi}$ are shown in Figs. 1 and 2.

This function satisfies the condition that

$$\sum_{k=-\infty}^{+\infty} \hat{\phi}(\omega + 2\pi k) = 1, \tag{4}$$

which is just a frequency-domain form of the fact that ϕ is a sampling function, i.e., $\phi(n) = \delta_{0,n}$ for any integer value n where $\delta_{0,n}$ is the Kronecker symbol,

$$\delta_{0,n} = \begin{cases} 1, & n = 0 \\ 0 & \text{otherwise.} \end{cases}$$

It should be observed that ϕ is not an orthogonal scaling function, but its translates do form a Riesz basis of their closed linear span.

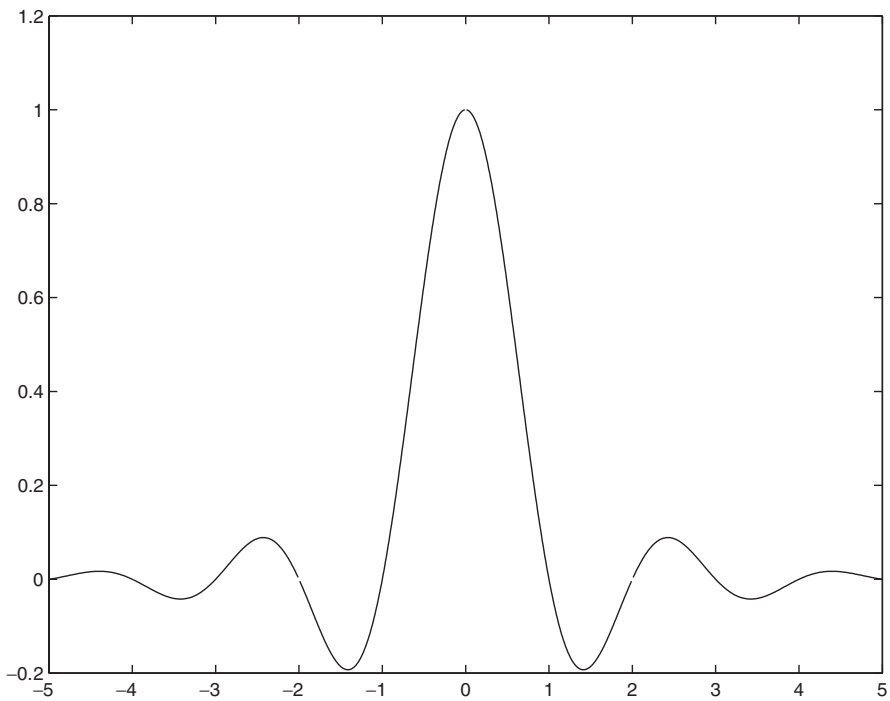

FIGURE 1 Graph of the raised-cosine spectrum function ϕ in the time domain.

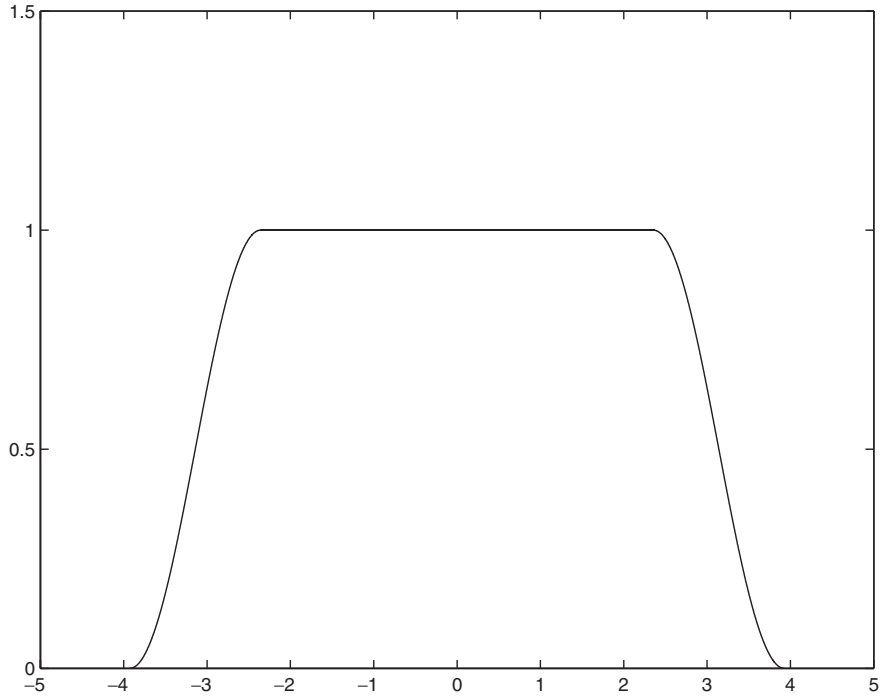

FIGURE 2 Graph of the raised–cosine spectrum function ϕ in the frequency domain.

To obtain an orthogonal scaling function we must take the square root in the frequency domain. One such root is given by

$$\hat{\phi}_1(\omega) = \begin{cases} 1, & 0 \le |\omega| \le \dfrac{3\pi}{4} \\ \dfrac{1}{2}\left[1 + e^{i(2\omega - (3\pi/2))}\right], & \dfrac{3\pi}{4} \le |\omega| \le \dfrac{5\pi}{4} \\ 0, & |\omega| > \dfrac{5\pi}{4} \end{cases}.$$

In the time domain ϕ_1 is

$$\phi_1(t) = \frac{\sin((3\pi/4)t) + \sin((5\pi/4)t)}{\pi t(2+t)}. \tag{5}$$

The graph of ϕ_1 is shown in Fig. 3; it also shares with $\phi(t)$ the sampling property $\phi_1(n) = \delta_{0,n}$, but has only quadratic decay.

3. RECONSTRUCTION ALGORITHM

We are now ready to introduce a reconstruction procedure based on the raised-cosine spectrum function defined above. We assume that the projection function $P_\theta(t) = R_\theta f(t)$ is known and will derive a procedure for recovering f.

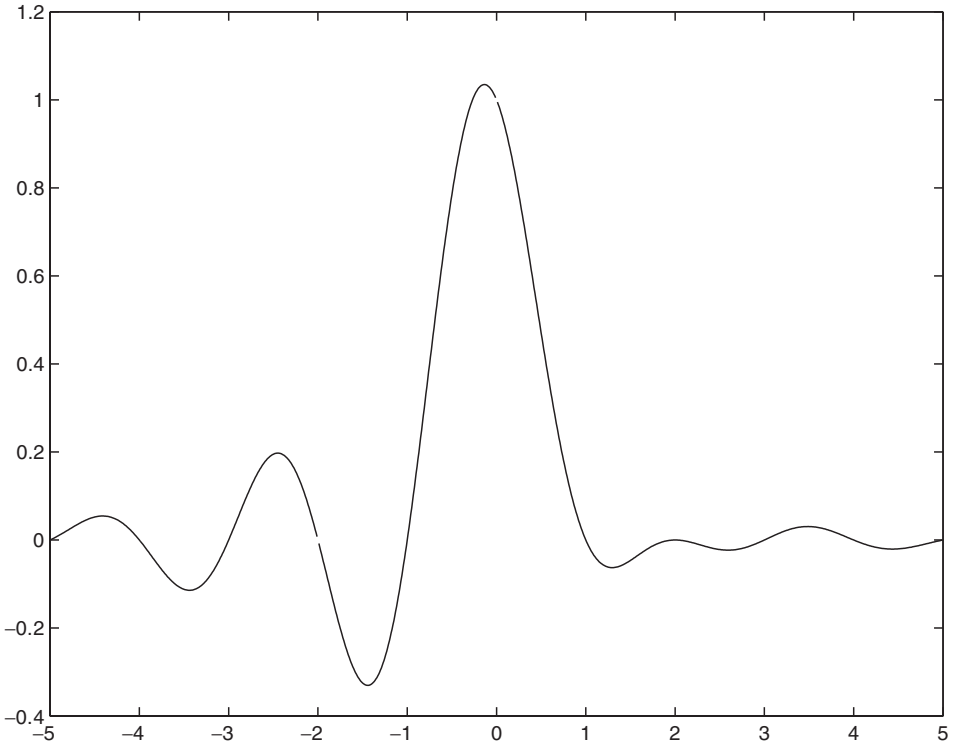

FIGURE 3 Graph of the raised-cosine scaling sampling function ϕ_1 in the time domain.

3.1 Procedure

We approximate the projection function $P_\theta(t)$ by the sampling series in ϕ at the scale of interest m:

$$P_{\theta,m}(t) = \sum_{n=-\infty}^{+\infty} P_\theta(n2^{-m})\phi(2^m t - n). \tag{6}$$

Then the filtered projection $Q_\theta(t) = (1/2\pi)\int_{-\infty}^{+\infty} \hat{\boldsymbol{P}}_\theta(\omega)|\omega|e^{i\omega t}d\omega$ can be approximated by

$$Q_{\theta,m}(t) = \frac{1}{2\pi}\sum_{n=-\infty}^{+\infty} P_\theta(n2^{-m}) \int_{-\infty}^{+\infty} \hat{\boldsymbol{\phi}}(\omega 2^{-m})|\omega|e^{i\omega(2^m t - n)2^{-m}}d\omega. \tag{7}$$

The inner integral in (7) is, in fact, taken only over a finite interval due to the finite support of $\hat{\boldsymbol{\phi}}$, so that we have

$$Q_{\theta,m}(t) = \frac{1}{2\pi}\sum_{n=-\infty}^{+\infty} P_\theta(n2^{-m})g_m(2^m t - n),$$

where the weight functions g_m are given by

$$g_m(2^m t - n) = \int_{-(5\pi/4)2^m}^{(5\pi/4)2^m} \hat{\phi}(\omega 2^{-m})|\omega| e^{i\omega(2^m t - n)2^{-m}} d\omega = 2^{2m+1} \int_0^{5\pi/4} \zeta \cos(\alpha\zeta)\hat{\phi}(\zeta) d\zeta, \quad (8)$$

where $\alpha = 2^m t - n$.

This last integral can be evaluated in closed form; depending on the value of α, we obtain the following weight coefficients:

$$2^{-2m} g_m(\alpha) = \begin{cases} \dfrac{17\pi^2}{16} - \dfrac{1}{2} & \alpha = 0, \\ \dfrac{3\pi}{16} - \dfrac{1}{2} & \alpha = \pm 2, \\ \dfrac{1}{\alpha^2(\alpha^2 - 4)} & \\ \times[\cos(5\pi/4\alpha)(12\alpha^2 - 16) & \\ + \sin(5\pi/4\alpha)(5\pi\alpha^3 - 20\pi\alpha) & \text{otherwise} \\ + \cos(3\pi/4\alpha)(12\alpha^2 - 16) & \\ + \sin(3\pi/4\alpha)(3\alpha^3\pi - 12\pi\alpha)] - 2/\alpha^2 & \end{cases} \quad (9)$$

where $\alpha = 2^m t - n$.

After g_m has been calculated, an approximation $f_m(x, y)$ to the object function $f(x, y)$ can be obtained as follows:

$$f_m(x, y) = \frac{1}{(2\pi)^2} \sum_{n=-\infty}^{+\infty} \int_0^{\pi} P_\theta(n2^{-m}) g_m(x\cos\theta + y\sin\theta)\, d\theta. \quad (10)$$

The formula (10) involves a one-time calculation of the weight coefficients $g_m(t)$ as given by (9). It also avoids both Fourier transforms and convolutions as compared to the usual reconstruction algorithms which do not.

In practice, the projection function $P_\theta(t)$ has compact support, so that the series in (10) is only a finite sum. It can be further discretized to obtain

$$f(x, y) \approx \frac{1}{(2\pi)^2} \frac{\pi}{K} \sum_{i=1}^{K} \sum_{n} P_{\theta_i}(n2^{-m}) g_m(x\cos\theta_i + y\sin\theta_i),$$

where K is the number of views and θ_i are the angles at which projections have been measured, $i = 1, \ldots, K$.

Since not all of the values of $x\cos\theta_i + y\sin\theta_i$ necessarily correspond to the values of t for which $g_m(t)$ in (9) are known, some kind of interpolation must be used. For our computer simulations, we have used linear interpolation.

3.2 Convergence Theorems

We now present some convergence results. We begin with the one for the approximation series in (6).

THEOREM 1 *Let $P_\theta(t)$ have compact support and $P_\theta(t) \in H^\alpha$ for some $\alpha > 1/2$ with $\|P_\theta(t)\|_\alpha \le C$ for some constant C. Then $P_{\theta,m}(t) \to P_\theta(t)$ uniformly for $\theta \in [0, 2\pi]$ and $t \in \mathbf{R}$ as $m \to \infty$ at the rate $\|P_{\theta,m} - P_\theta\|_\infty = O\left(2^{-m(\alpha-1/2)}\right)$.*

The proof is given in the appendix.

A couple of remarks would be in place.

1. It should be noticed that the proof of Theorem 1 does not depend on choice of $\phi(t)$. That means that, in fact, any other bandlimited function ϕ satisfying $\sum_{k=-\infty}^{+\infty} \hat{\phi}(\omega + 2\pi k) = 1$ and $\hat{\phi}(2^{-m}\omega) = 1$ for $|\omega| \le \omega_0$ for some constant ω_0 can be used in place of the raised-cosine spectrum function. For example, ϕ could be chosen to be equal to ϕ_1 in (5). In fact, $\hat{\phi}$ can be chosen to be C^∞ as in Meyer's original formulation [14]. In this case it does not have a closed form, however.
2. Ideally, real projection data need not be smooth, i.e., $P_\theta(t)$ need not be in H^α for $\alpha > 1/2$. In fact one would expect that some discontinuities in $f(x, y)$ would lead to discontinuities in $P_\theta(t)$. But this is usually not the case with real data since many averaging operations are involved. Real data should be bandlimited since no real process allows arbitrarily large frequencies, but it is frequently corrupted by wideband noise.

Similar result can be obtained for the image function itself approximated by the series (10).

THEOREM 2 *Let $P_\theta(t)$ have compact support and $P_\theta(t) \in H^\alpha$ for some $\alpha > 3/2$ with $\|P_\theta(t)\|_\alpha \le C$ for some constant C. Then the sampling series in* (10) *converges uniformly to $f(x, y)$ as $m \to \infty$ for $(x, y) \in \mathbf{R}^2$ at the rate $O(2^{-m(\alpha-(3/2))})$.*

The proof is similar to that of Theorem 1 as is mentioned.

Remark If we are interested in the convergence of $P_{\theta,m}(t)$ to $P_\theta(t)$ but not the rate, we do not need the hypothesis that $P_\theta(t) \in H^\alpha$ for any α. Rather all we need is that $\hat{P}_\theta \in L^1$. Then we have $P_{\theta,m} \to P_\theta$ uniformly on $\mathbf{R}$ by the dominated convergence theorem. Similarly, for the uniform convergence of $f_m(x, y)$ to $f(x, y)$ we need only require that $\omega \hat{P}_\theta(\omega) \in L^1$. Both requirements are met in practical situation since $\hat{f}$ and $\hat{P}_\theta$ would be rapidly decreasing.

4. COMPUTER IMPLEMENTATION

Our reconstruction algorithm was tested on the well-known Shepp–Logan "head phantom" [16] which is a standard test for the CT algorithms. This image model consists of 10 ellipses with various gray levels inside them (Fig. 4).

The following description of this model can be found in [16]: "In an attempt to be consistent with known facts about the human head, the skull in the figure is about twice as dense as the interior tissue and is thicker at the forehead. The ventricles filled with spinal fluid (water) are least dense (1.0), while gray matter has density 1.02 and fills the interior of the head except for tumors (1.03)...." For this model,

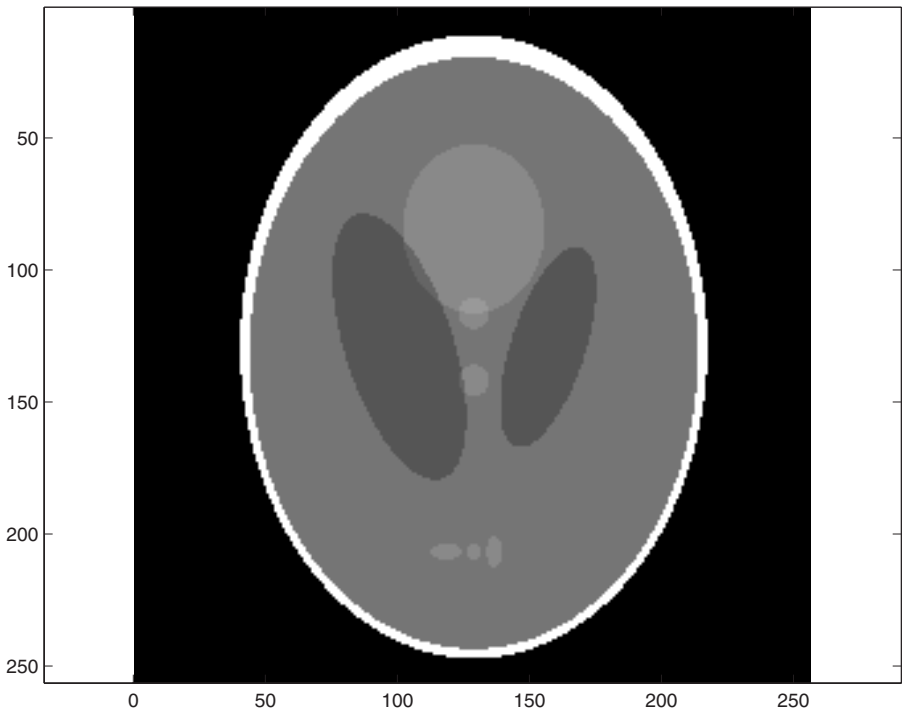

FIGURE 4 The actual Shepp–Logan head phantom.

the range of gray scale values is [0.0, 2.0] and the features we are interested in have values close to 1.0. It should be noticed that gray levels of these features have very close values with only a 4% variation inside the skull, the highest point being the tumor (1.04) between ventricles (1.0). This makes the problem of recovery of the object function $f(x, y)$ from its projections even more challenging.

Since the Radon transform is linear, analytic formulae can be obtained for the projection function of the Shepp–Logan image since it is a superposition of gray levels of 10 ellipses mentioned above.

In order to apply our convergence results, we need to discuss the regularity of the Shepp–Logan projection function. This may be found by considering an image consisting of a unit circle with density 1 inside and 0 outside. The projection function of this object is

$$P_\theta(t) = \begin{cases} \sqrt{1-t^2}, & |t| \le 1 \\ 0, & |t| > 1. \end{cases}$$

Its Fourier transform is given by

$$\hat{P}_\theta(\omega) = \sqrt{\pi}\Gamma\left(\frac{3}{2}\right)\frac{2}{|\omega|}J_1(|\omega|),$$

where $J_1(x)$ is the Bessel function of order one. Since for large values of x we can approximate $J_1(x)$ by $\sqrt{2/\pi x}\cos(x - (3\pi/4))$, we obtain $\hat{P}_\theta(\omega) \approx |\omega|^{-(3/2)}$ and,

therefore, $\hat{P}_\theta^2(\omega)(1+\omega^2)^\alpha \approx 1/\omega^{3-2\alpha}$ for large ω. Thus, the projection function of this circle is in the Sobolev space H^α when $3-2\alpha > 1$, i.e., when $\alpha < 1$. This conclusion can be extended to ellipses and by superposition to the Shepp–Logan projection function. It follows that the hypothesis of Theorem 1 ($\alpha > 1/2$) is satisfied and that of Theorem 2 ($\alpha > 3/2$) is not. This does not, of course, imply that convergence fails in that theorem since the conditions are sufficient and not necessary. In fact, in all cases experimental results were much better than one would expect from these theorems. Given real data, one would also expect that the images are smoother than for this case since a real object function would be smoother than the Shepp–Logan image function.

Assume that the projection data were sampled at N evenly spaced points over the interval $[-1, 1]$. Since we are using the sampling approximation (6) with a sampling interval $T = 2^{-m}$, this implies that we must have $N = 2/T = 2^{m+1}$, or

$$m = [\log_2 N - 1]. \tag{11}$$

Thus, the scale of interest m is directly related to the number of points at which projections are known.

In the following we summarize our reconstruction algorithm

1. *Filtering* For each point $t_n = nT$, $n = -(N/2), -(N/2)+1, \ldots, (N/2)-1$, we calculate the corresponding value of the weight function $g_m(nT)$ accordingly to (9). Note that g_m does not depend on the angle at which a projection is measured except through its argument. Therefore, g_m can be evaluated in advance (i.e., before the backprojection step is performed). We then generate the corresponding filtered projection

$$Q_{\theta_i}(jT) = \frac{1}{2\pi} \sum_{n=-(N/2)}^{(N/2)-1} P_{\theta_i}(n2^{-m}) g_m(jT), \qquad j = -\frac{N}{2}, \ldots, \frac{N}{2} - 1,$$

for each angle $\theta_i, i = 1, \ldots, K$.

2. *Backprojection* We use discrete approximation to the integral $f(x, y) = (1/2\pi) \times \int_0^\pi Q_\theta(t)\, d\theta$, $t = x\cos\theta + y\sin\theta$, to recover the image function:

$$f(x, y) = \frac{1}{2\pi} \frac{\pi}{K} \sum_{i=1}^{K} Q_{\theta_i}(x\cos\theta_i + y\sin\theta_i), \tag{12}$$

where K is the number of angles θ_i at which projections are known. Since some of the values of $x\cos\theta_i + y\sin\theta_i$ may not be equal to any of the points jT for which P_θ was measured, interpolation is needed. We use linear interpolation, if necessary, to get these values.

The computational complexity of this algorithm similar to that of the standard backprojection algorithm [16]. Since the values of the weight functions $g_m(t)$ can be precomputed and stored, it takes N^2 multiplications to obtain the filtered projection $Q_{\theta_i}(jT)$ for all sampling points $jT, j = -(N/2), \ldots, N/2 - 1$, and each angle θ_i, $i = 1, \ldots, K$. These filtered projections are backprojected accordingly to (12). Hence, the total complexity is $K(N^2 + C_l)$ where C_l is the complexity of linear interpolation used as a part of backprojection step.

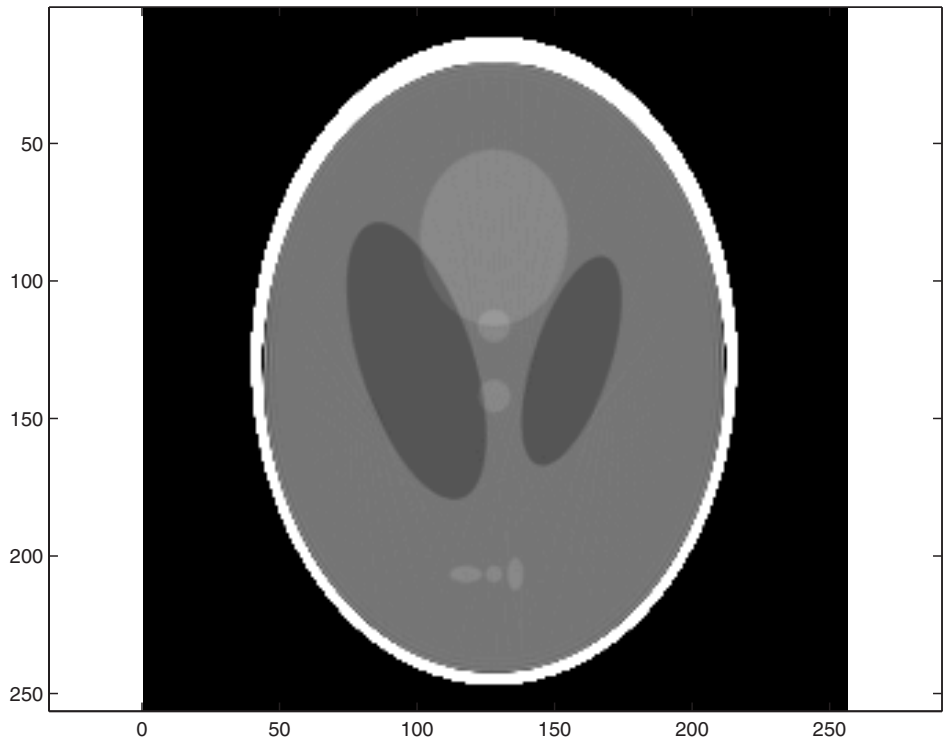

FIGURE 5 The reconstructed Shepp–Logan image.

Remark Steps 1 and 2 above are essentially the same ones as in the standard backprojection algorithm described in the Introduction. This means that the raised-cosine based algorithm could be implemented on current CT machines and only few adjustments are needed. However, our algorithm avoids convolution and therefore should require fewer calculations. In the standard approximation, the integral used to obtain $Q_\theta(t)$ is merely truncated. This means that $Q_\theta(t)$ is approximated by the Fourier transform of a discontinuous function which results in a very slow convergence as $t \to \pm\infty$. In our case the discontinuity is smoothed and should give better convergence.

We reconstructed the 256×256 pixel image of the Shepp–Logan phantom from $K = 256$ projections with $N = 256$ points in each projection. Accordingly to (11), the finest scale of interest is $m = 7$. The reconstructed image is shown in Fig. 5.

The computer program was done in C++. The weight coefficients g_m were calculated accordingly to (9). In actual implementation, those values would be precomputed and stored. Linear interpolation was used for the whole sum in (12).

SUMMARY

Our algorithm avoids integration and uses only precomputed coefficients in the filtering step. This, coupled with the fact that the complexity is no greater than traditional methods, should give it an advantage over them. The quality of the image in the test case is as good or better than other methods.

References

[1] A. Aldroubi (1996). Oblique projections in atomic spaces. *Proc. Amer. Math. Soc.*, **124**, 2051–2060.
[2] C. Berenstein, F. Rashid-Farrokhi, K.J.R. Liu and D. Walnut (1997). Wavelet-based multiresolution local tomography. *IEEE Trans. Image Proc.*, **6**, 1412–1430.
[3] C. Berenstein and D. Walnut (1994). Local inversion of the Radon transform in even dimensions. In: S. Gindikin and P. Michor (Eds.), *75 Years of Radon Transform*, pp. 38–58. International Press, Cambridge, MA.
[4] Z.H. Cho, J.P. Jones and M. Singh (1993). *Foundations of Medical Imaging*. John Wiley and Sons, New York.
[5] I. Daubechies (1992). *Ten Lectures on Wavelets*. SIAM, Philadelphia.
[6] I. Daubechies (1988). Orthonormal bases of compactly supported wavelets. *Comm. Pure Appl. Math.*, **41**, 909–996.
[7] S.R. Deans (1991). The Radon transform and some of its applications. Reprinted Edn., Krieger, Malabar, FL.
[8] J. DeStefano and T. Olson (1992). Wavelet localization of the radon transform. *IEEE–SP Int. Symp. Time–Frequency and Time–Scale Analysis*. Victoria, BC, Canada.
[9] D. Donoho (2000). Orthonormal ridgelets and linear singularities. *SIAM J. Math. Anal.*, **31**, 1062–1099.
[10] M. Holschneider (1991). Inverse Radon transforms through inverse wavelet transforms. *Inverse Problems*, **7**, 853–861.
[11] A.J. Jerri (1977). The Shannon sampling theorem – its various extensions and applications: a tutorial review. *Proc. IEEE*, **65**, 1565–1596.
[12] A.C. Kak and M. Slaney (1988). Principles of computerized tomographic imaging. *IEEE Press*, New York.
[13] G. Kaiser and R. Streater (1992). Windowed Radon transforms. In: C.K. Chui (Ed.), *Wavelets: A Tutorial Theory and Applications*, pp. 399–441. Academic Press, New York.
[14] Y. Meyer (1990). *Ondelettes et Operateurs*. Hermann, Paris.
[15] C.E. Shannon (1949). Communication in the presence of noise. *Proc. IRE*, **37**, 10–21.
[16] L.A. Shepp and B.F. Logan (1974). The Fourier reconstruction of a head section. *IEEE Trans. Nucl. Sci.*, NS–21, 21–43.
[17] M. Unser, A. Aldroubi and M. Eden (1991). Fast B-spline transforms for continuous image representation and interpolation. *IEEE Trans. Patt. Recog. and Mach. Intell.*, **13**, 277–285.
[18] M. Unser, A. Aldroubi and M. Eden (1993). B-spline signal processing: Part II – Efficient design and applications. *IEEE Trans. Sgnal Proc.*, **41**, 834–848.
[19] P.P. Vaidyanathan (2001). Generalizations of the sampling theorems: seven decades after Nyquist. *IEEE Trans. Circuits and Systems-I*, **48**, 1094–1109.
[20] D. Walnut (1992). Applications of Gabor and wavelet expansions to the Radon transform. In: J. Byrnes *et al.* (Eds.), *Probabilistic and Stochastic Methods in Analysis, with Applications*, pp. 187–205. Kluwer Academic Publishers, Boston.
[21] G.G. Walter (1994). *Wavelets and Other Orthogonal Systems with Applications*. CRC Press, Boca Raton, FL.
[22] G.G. Walter (1992). A sampling theorem for wavelet subspaces. *IEEE Trans. Info. Theory*, **38**, 881–884.
[23] G.G. Walter and J. Zhang (1998). Orthonormal wavelets with simple closed-form expressions. *IEEE Trans. Signal Proc.*, **46**, 2248–2251.

APPENDIX

Proof of Theorem 1 We first estimate the difference between the projection function $P_\theta(t)$ and its approximating series $P_{\theta,m}(t) = \sum_{n=-\infty}^{+\infty} P_\theta(n2^{-m})\phi(2^m t - n)$ in the frequency domain. We have

$$\begin{aligned}
\hat{P}_{\theta,m}(\omega) &= \sum_{n=-\infty}^{+\infty} 2^{-m} P_\theta(n2^{-m})\hat{\phi}(\omega 2^{-m}) e^{-i\omega n 2^{-m}} \\
&= \sum_{n=-\infty}^{+\infty} \frac{1}{2\pi} \int_{-\infty}^{+\infty} \hat{P}_\theta(\zeta) e^{in2^{-m}\zeta} d\zeta \; 2^{-m}\hat{\phi}(\omega 2^{-m}) e^{-i\omega n 2^{-m}} \\
&= \int_{-\infty}^{+\infty} \hat{P}_\theta(\zeta) \left[\frac{1}{2\pi} \sum_{n=-\infty}^{+\infty} e^{in2^{-m}(\zeta-\omega)} \right] 2^{-m}\hat{\phi}(\omega 2^{-m})\, d\zeta,
\end{aligned} \tag{13}$$

where we used $P_\theta(n2^{-m}) = 1/(2\pi)\int_{-\infty}^{+\infty} \hat{P}_\theta(\zeta)e^{in2^{-m}\zeta}\,d\zeta$. But the sum $(1/2\pi)\sum_{n=-\infty}^{+\infty} e^{in2^{-m}(\zeta-\omega)}$ is exactly $\delta^*(2^{-m}(\omega-\zeta))$, where δ^* is the periodic δ function, $\delta^* = \sum_{n\in\mathbf{Z}} \delta(x+2\pi n)$. This is an element of the dual space S' of S. Since P_θ has compact support, $\hat{P}_\theta$ is analytic and in $L^1(\mathbf{R})$. Hence, the integral can be interpreted as a convolution $\langle \delta^*(2^{-m}(\omega-\bullet)), \hat{P}_\theta\rangle$. Therefore, by using the filtering property of δ, (13) can be formally rewritten as

$$\begin{aligned}\hat{P}_{\theta,m}(\omega) &= \int_{-\infty}^{+\infty} \hat{P}_\theta(\zeta)\delta^*(2^{-m}(\omega-\zeta))\,2^{-m}\,d\zeta\,\hat{\phi}(2^{-m}\omega)\\ &= \sum_{k=-\infty}^{+\infty} \hat{P}_\theta(\omega+2^{m+1}\pi k)\hat{\phi}(2^{-m}\omega).\end{aligned} \tag{14}$$

This formula could also be obtained from the Poisson summation formula. Thus, $E = \hat{P}_{\theta,m} - \hat{P}_\theta$ has the form $E(\omega) = \hat{P}_\theta(\omega)[\hat{\phi}(2^{-m}\omega - 1)] + \sum_{k\neq 0} \hat{P}_\theta(\omega + 2^{m+1}\pi k)\hat{\phi}(2^{-m}\omega)$. Hence, the integral $\int_{-\infty}^{+\infty} |E(\omega)|\,d\omega$ satisfies

$$\begin{aligned}\int_{-\infty}^{+\infty} |E(\omega)|d\omega &= \int_{-\infty}^{+\infty} |\hat{P}_{\theta,m}(\omega) - \hat{P}_\theta(\omega)|\,d\omega\\ &\leq \int_{-\infty}^{+\infty} |\hat{P}_\theta(\omega)||\hat{\phi}(2^{-m}\omega) - 1|\,d\omega\\ &\quad + \int_{-\infty}^{+\infty} \hat{\phi}(2^{-m}\omega)\sum_{k\neq 0}|\hat{P}_\theta(\omega+2\pi k2^m)|\,d\omega.\end{aligned} \tag{15}$$

The second integral in (15) is

$$\begin{aligned}&\int_{-\infty}^{+\infty} \hat{\phi}(2^{-m}\omega)\left(\sum_{k=-\infty}^{k=+\infty} |\hat{P}_\theta(\omega+2\pi k2^m)| - |\hat{P}_\theta(\omega)|\right)d\omega\\ &= \int_{-\infty}^{+\infty}\left[\sum_{k=-\infty}^{+\infty} \hat{\phi}(2^{-m}(\omega-2\pi k2^m))|\hat{P}_\theta(\omega)| - \hat{\phi}(2^{-m}\omega)|\hat{P}_\theta(\omega)|\right]d\omega\\ &= \int_{-\infty}^{+\infty} |\hat{P}_\theta(\omega)||\hat{\phi}(2^{-m}\omega) - 1|d\omega.\end{aligned} \tag{16}$$

Here we have used the fact that $\sum_{k=-\infty}^{+\infty} \hat{\phi}(\omega + 2\pi k) = 1$.

Since both integrals in (15) are dominated by $\int_{-\infty}^{+\infty} |\hat{P}_\theta(\omega)||\hat{\phi}(2^{-m}\omega) - 1|d\omega$ and since $\hat{\phi}(2^{-m}\omega) = 1$ for $|2^{-m}\omega| \leq 3\pi/4$, it follows that

$$\int_{-\infty}^{+\infty} |\hat{P}_{\theta,m}(\omega) - \hat{P}_\theta(\omega)|d\omega \leq 2\int_{-\infty}^{-(3\pi/4)2^m} |\hat{P}_\theta(\omega)|d\omega + 2\int_{(3\pi/4)2^m}^{+\infty} |\hat{P}_\theta(\omega)|d\omega.$$

Since $P_\theta(t)$ is in the Sobolev space H^α, we have

$$\begin{aligned}\int_{(3\pi/4)2^m}^{+\infty} |\hat{P}_\theta(\omega)|\, d\omega &= \int_M^{+\infty} \frac{|\hat{P}_\theta(\omega)|}{(1+\omega^2)^{\alpha/2}} (1+\omega^2)^{\alpha/2} d\omega \\ &\le \left[\int_M^{+\infty} \frac{1}{(1+\omega^2)^\alpha} d\omega \int_{-\infty}^{+\infty} |\hat{P}_\theta(\omega)|^2 (1+\omega^2)^\alpha d\omega\right]^{1/2} \\ &\le CM^{(1-2\alpha)/2} \|P_\theta\|_\alpha,\end{aligned}$$

where $M = (3\pi/4)2^m$. Similarly, we can obtain the same estimates for the integral $\int_{-\infty}^{-(3\pi/4)2^m} |\hat{P}_\theta(\omega)| d\omega$. Thus, the integral $\int_{-\infty}^{+\infty} |E(\omega)| d\omega$ satisfies

$$\int_{-\infty}^{+\infty} |E(\omega)| d\omega \le 4C \|P_\theta\|_\alpha (2^m)^{(1-2\alpha)/2} \left(\frac{3\pi}{4}\right)^{(1-2\alpha)/2}.$$

Since the norm $\|P_\theta\|_\alpha$ is uniformly bounded for all $\theta \in \mathbf{R}$, we have for $\alpha > 1/2$

$$\int_{-\infty}^{+\infty} |\hat{P}_{\theta,m}(\omega) - \hat{P}_\theta(\omega)| d\omega = O\big(2^{-m(\alpha-(1/2))}\big).$$

We obtain

$$\sup |P_{\theta,m}(t) - P_\theta(t)| \le \frac{1}{2\pi} \int_{-\infty}^{+\infty} |\hat{P}_{\theta,m}(\omega) - \hat{P}_\theta(\omega)| d\omega \quad \text{for } \theta,\ t \in \mathbf{R},$$

since $P_\theta(t) = 1/2\pi \int_{-\infty}^{+\infty} \hat{P}_\theta(\omega) e^{i\omega t} d\omega$. Thus, the series $P_{\theta,m}(t)$ converges uniformly to $P_\theta(t)$ as $m \to \infty$ at the rate $O(2^{-m(\alpha-1/2)})$, which completes the proof.

A few modifications of the derivation above with t replaced by $x\cos\theta + y\sin\theta$ will produce the proof of Theorem 2.